*Article*

# Study on Microstructure and Mechanical Property in Mg-Gd-Y Alloy by Secondary Extrusion Process

Jianhua Liu, Jie Sun *, Qingqiang Chen [ID], Laixiao Lu and Yanhua Zhao

School of Mechanical and Electronic Engineering, Shandong Jianzhu University, Jinan 250101, China; ljh@sdjzu.edu.cn (J.L.); 13770@sdjzu.edu.cn (Q.C.); lulaixiao@sdjzu.edu.cn (L.L.); zyh@sdjzu.edu.cn (Y.Z.)
* Correspondence: sunjie20@sdjzu.edu.cn; Tel./Fax: +86-0531-8636-7021

**Abstract:** Extruded Mg-Gd-Y alloy tubes were obtained by using cast ingot and extruded bar billets. Microstructure and mechanical properties were also studied with two different cooling methods: air cooling and water cooling. The result shows that by using an extruded bar as billet extruded tubes achieves higher elongation comparing to using cast ingots due to favored texture for the activation of basal slip. Using the water-cooling method, extruded tubes achieve a higher yield strength compared to the air cooling method due to their fine grain size. Using cast ingot billets and the water-cooling method, the elongation is only 6% due to large unrecrystallized grains caused by inhomogeneous deformation and unfavored texture for the activation of basal slip. Using the extruded bar billet and the water-cooling method, the tube has uniformed small grains and much more randomized texture caused by the inhibition of preferred grain growth process. The highest texture intensity is only 1.852 in this kind of tube. Both high yield strength (195.3 MPa) and high elongation (23.9%) are achieved in this tube.

**Keywords:** rare-earth magnesium alloy; secondary extrusion; texture; mechanical property

## 1. Introduction

Wrought magnesium alloys attract significant interest in fields such as automobiles, aircraft and space machinery due to their high strength properties combined with quite low density [1,2]. Magnesium extrusions, especially hollow sections, could further offer attractive mass-saving opportunities for automotive light weighting with potential applications in instrument panel beams, seat frames, roof frames, bumper beams, radiator support, engine cradles and subframes [3]. It is, therefore, meaningful to produce high-strength magnesium alloy tubes as an alternative to aluminum and steel. However, significant challenges remain in magnesium extrusions, such as their limited formability, which is related to their low ductility at room temperature [4–7].

Research to date suggests that texture modification and grain refinement are the most promising approaches for improving the ductility of wrought magnesium alloys. Earlier research suggested that magnesium alloys containing yttrium (Y) [8–10], neodymium (Nd) [11–13], Cerium (Ce) [14,15] and Gadolinium (Gd) [16,17] developed a more random texture during extrusion. Recent work also confirmed that small additions of rare earth elements can improve the mechanical properties of magnesium extrusions and sheets via grain refinement and weakening of texture [16]. Our recent work reported a significant increase in elongation in pure magnesium due to the addition of only 1% Gd in rolling sheets, and attributed this increase to a change in the texture that favors basal slips [16].

Although the RE addition could alter the texture and improve the ductility, the Mg-RE alloy with a low content of the RE element appears low yield strength, such as ZE10 (135 MPa) [18,19] and Mg-1Gd (130 MPa) [16]. The strength of the Mg-Zn-Ce and Mg-Zn-Y system alloys are still not enough for the automotive application, such as for door beams. The hardening with other element addition and heat treatment should be involved to achieve the precipitate strengthening.

Mg-8%Gd-3%Y alloy (GW83) is a potential alloy with a random texture and precipitation, and the alloy shows good strength and better yield symmetry in our previous study. The formability and the final mechanical properties of the alloy tube are dependent on the initial microstructure and processing parameters. In this study, Mg-8%Gd-3%Y (GW83) alloy square tubes with internal stiffener were prepared by extrusion. Additionally, the effect of the initial microstructure and cooling rate after extrusion on the microstructure evolution and mechanical properties was investigated. The aim is to develop the process for high-performance tubes in automobiles.

## 2. Experiment

The material employed in the present work is Mg-8Gd-3Y alloy. There are two groups of initial billets used in this extrusion, which are as-cast billets and extruded bars. The as-cast billets with cylinder shapes of 100 mm diameter and 250 mm length are from continuous casting. The extruded bar with the same size was extruded by using a cast billet with diameter of 180 mm. Homogenization was performed before the extrusion process at 400 °C for 1h. Additionally, thereafter, the cast ingot billets and the extruded bars are used as the initial materials for extrusion of the square tubes with internal stiffener. Figure 1 shows the designed dimensions of the final extrusion tube. In addition, different cooling methods (air cooling and water cooling) and extruded temperature were utilized in the extrusion of the square tubes. In this study, the tube using cast ingot billets and air cooling is named CA, the tube using cast ingot billets and water cooling is named CW, the tube using extruded bars and air cooling is named EA and the tube using extruded bars and water cooling is named EW. Table 1 shows the samples with the according extrusion parameters. The appearance of the extruded tube is shown in Figure 1b. It can be seen that the appearance of these tubes is quite good, and the dimension is fit for the designed value.
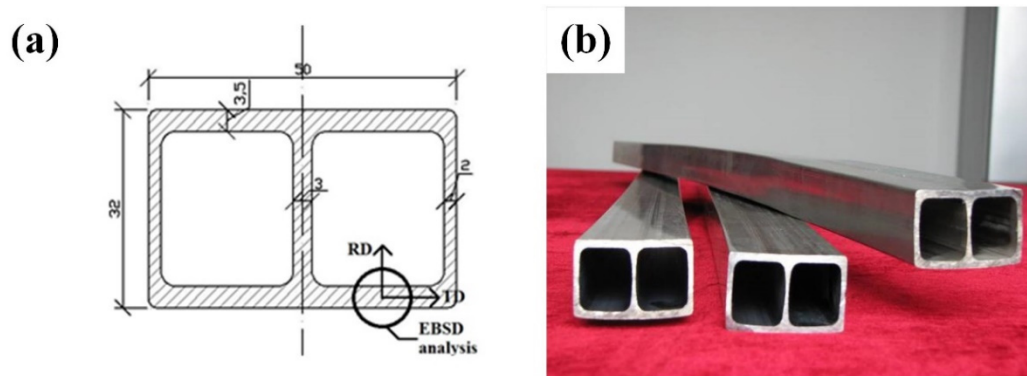


**Figure 1.** (**a**) Designed dimensions of extrusion tube, (**b**) outline quality of the extruded tubes.

**Table 1.** Extrusion parameters of experimental alloys.

| | Billet | Temperature (°C) | | Cooling Method |
| --- | --- | --- | --- | --- |
| | | Mould | Billet | |
| CA | Cast ingot | 400 | 390 | Air |
| CW | Cast ingot | 400 | 390 | Water |
| EA | Extruded bar | 400 | 390 | Air |
| EW | Extruded bar | 400 | 390 | Water |

The initial microstructure and texture were examined by optical microscopy (OM), scanning electron microscope (SEM) and electron backscatter diffraction (EBSD). Additionally, the sampling location of EBSD scanning is also shown in Figure 1. Radial direction (RD) and tangential direction (TD) are defined in Figure 1a. OM and SEM samples were etched in the Acetic–Picral solution (10 mL acetic acid, 4.2 g picric acid, 10 mL distilled water, and 70 mL ethanol (96%)) for 15 s. EBSD samples were mechanically polished and

chemically etched in a solution of 5 mL nitric acid, 15 mL acetic acid, 20 mL water and 60 mL ethanol for 2 s to remove the surface residual stress. The EBSD analysis was carried using a Quanta 250 SEM equipped with a TSL$^{TM}$ EBSD camera and an OIM software package. The EBSD scanning process was carried out at a step size of 1 µm with the voltage of 20 kV and current of 107 nA.

The texture was analyzed by the TSL OIM data acquisition and analysis software package. Uniaxial tension tests on Mg-Gd-Y alloy tubes were conducted on the ZWICK mechanical testing machine at an ambient temperature along the extrusion direction (ED). To ensure the repeatability of stress–strain tests, three samples were tested, and the average values and standard deviations of the tensile properties are shown in Figure 6.

## 3. Results

### 3.1. Microstructure

The microstructures of initial billets are shown in Figure 2 and show homogeneous distribution in grain size, but the cast ingot billet shows a big grain size about 200 µm and the extruded bar shows a fine grain size about 25 µm.
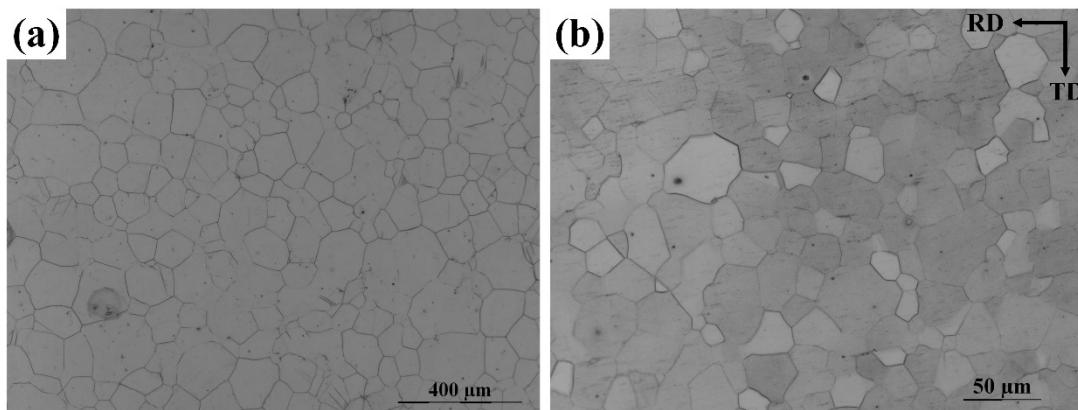


**Figure 2.** Microstructure of the billets (**a**) cast ingot (**b**) extruded bar.

Microstructures of the extruded tubes in four extrusion process are shown in Figure 3. Fully recrystallized grains can be found in most tubes except the CW tube. A large fraction of unrecrystallized grains is shown in the CW tube with different morphologies. Some grains are formed in long strips and some are formed in a square shape with a large grain size. This indicates that the extrusion process is not homogeneous at the grain size level. Distribution of grains with different grain size can also be seen in the EA and EW tubes (Figure 3c,d) but these grains are all recrystallized grains due to the fine grain size of the initial extrusion billets.

Grain size is different in these tubes (shown in Table 2). CA and EA tubes using air cooling show a grain size of 26 µm. CW and EW tubes using water cooling show a grain size of 8 µm and 6.3 µm, respectively. Therefore, grain refinement is effective by using the water-cooling method after the extrusion process.

In addition, a few small cuboidal particles with a mean size of about 1–2 µm can be observed along the extrusion direction (ED) (Figure 4a) and the composition of the particle detected by EDS is shown in Figure 4b. It is a kind of typical particle precipitated during the extrusion process in Mg-Gd-Y alloys and the total volume fraction of particles is quite small in each tube.
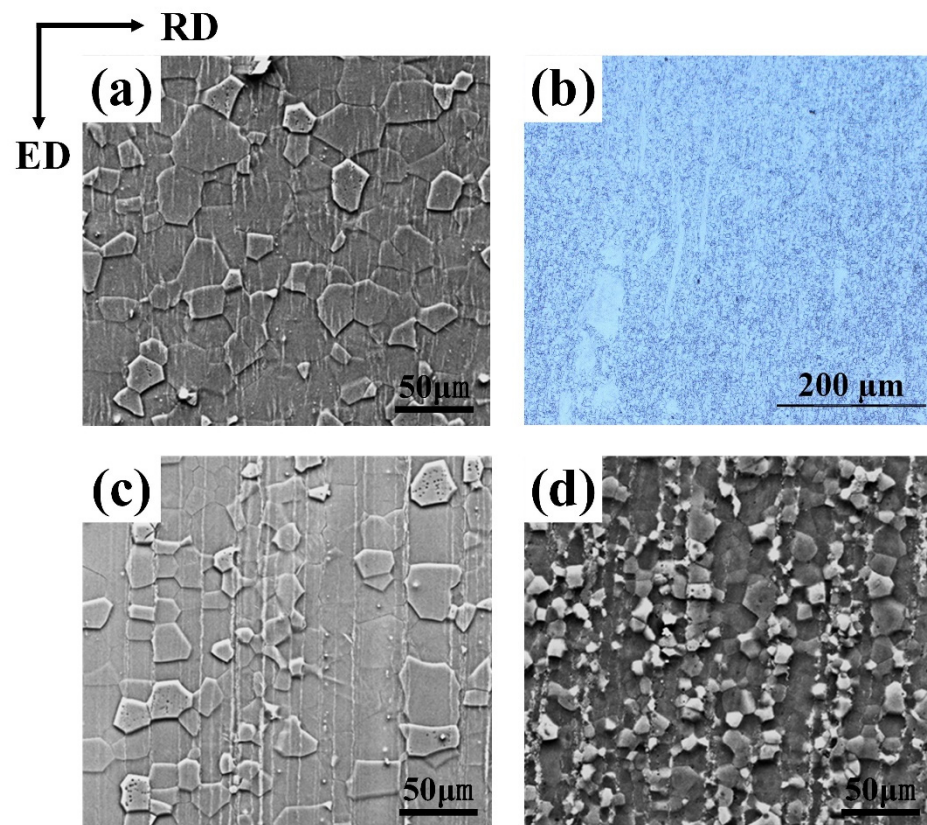
**Figure 3.** Microstructure of the extruded tubes (RD–ED section), (**a**) CA tube, (**b**) CW tube, (**c**) EA tube, (**d**) EW tube.

**Table 2.** Grain size of different extrusion tubes.

|  | Grain Size (µm) |
|---|---|
| CA | 26 |
| CW | 8 |
| EA | 26 |
| EW | 6.3 |



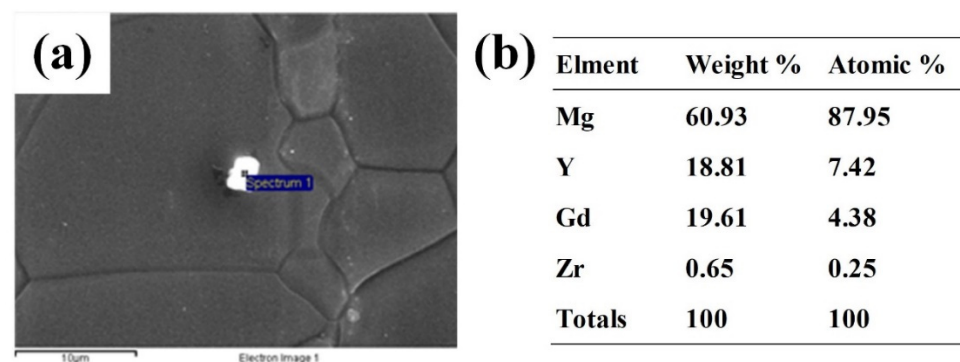| Elment | Weight % | Atomic % |
|---|---|---|
| Mg | 60.93 | 87.95 |
| Y | 18.81 | 7.42 |
| Gd | 19.61 | 4.38 |
| Zr | 0.65 | 0.25 |
| Totals | 100 | 100 |

**Figure 4.** (**a**) Microstructure of the second phase in the extruded tube, (**b**) EDS analysis of the second phase.

*3.2. Mechanical Property*

Stress–strain curves of all tubes are shown in Figure 5 and comparisons of yield stress and elongation are shown in Figure 6. CW and EW tubes using water cooling show higher yield stress than tubes using air cooling. This is due to the fine grain size in CW and EW tubes.
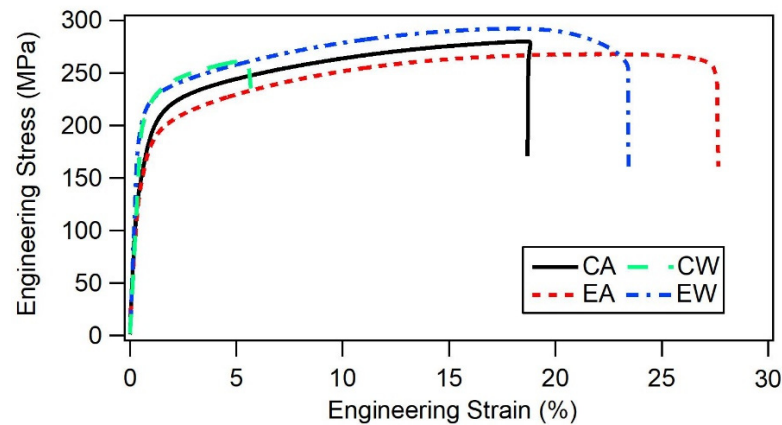
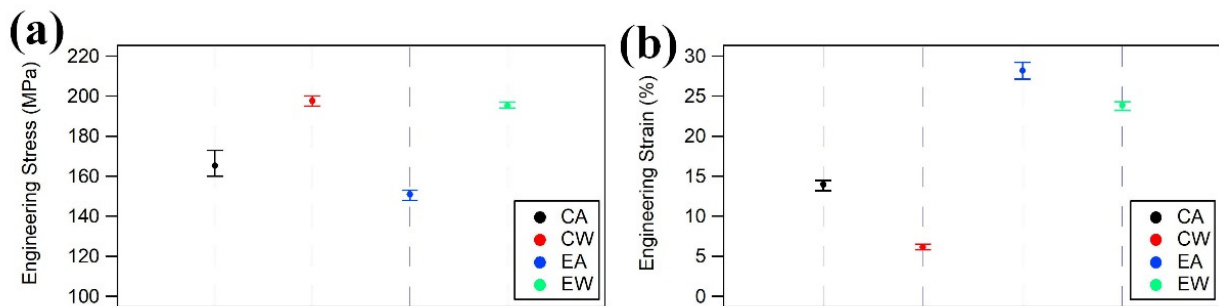**Figure 5.** Stress–strain curves of different tubes (tension along ED).

**Figure 6.** Comparison of mechanical property in different tubes, (**a**) yield stress, (**b**) elongation.

EA and EW tubes using the extruded bar as billet show higher elongation than tubes using cast ingots as billet. The elongations of EA and EW tubes are 28.2% and 23.9%, respectively. The CW tube shows the lowest elongation of 6%, which may be caused by the unrecrystallized grains with a large grain size.

*3.3. Texture*

The PF maps of all tubes are shown in Figure 7. The texture intensity of all tubes is weakened compared to traditional extruded magnesium alloys with obvious fiber texture. The highest texture intensity is 3.898 shown in EA tube. The lowest texture intensity is 1.825 shown in the EW tube. In typical fiber textures, the c-axis is approximately perpendicular to the extrusion direction. In the extruded Mg-Gd-Y alloy shown in this work, peaks on the (0001) pole figure shows an obvious deflection from the RD component. The peak intensity point in PF maps shows tilt from RD to ED at different degrees.

Inverse Pole Figures of different tubes are shown in Figure 8. Tubes produced by the water-cooling method show a peak around the <10-10> component which is caused by the deformation process. Tubes produced by the air-cooling method show a peak at the <2-1-10> component which is caused by the slow cooling rate and annealing effect.
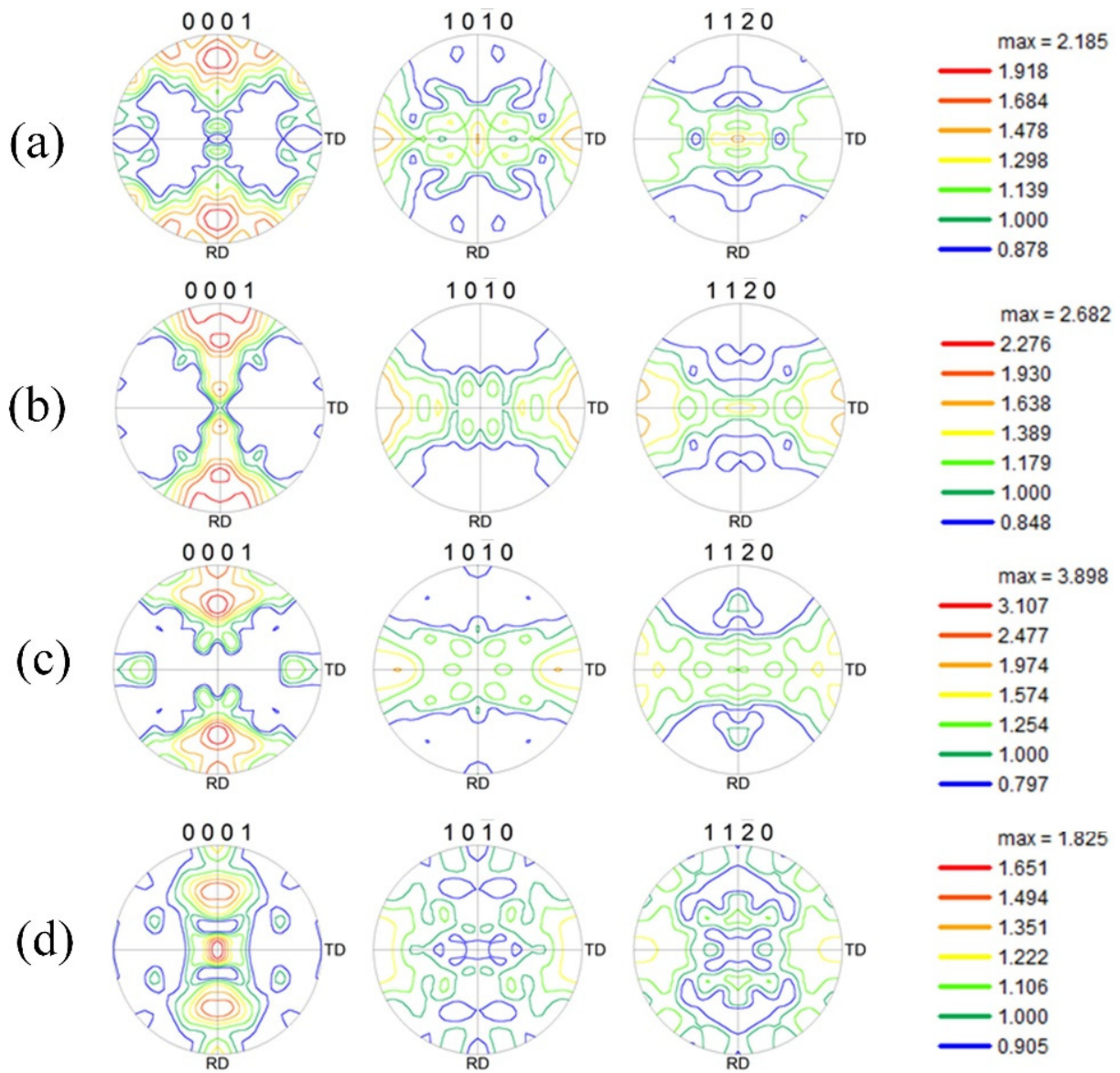
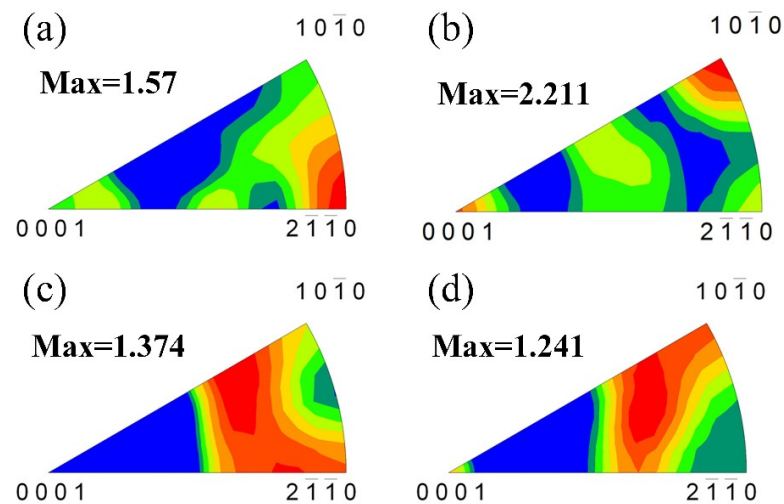**Figure 7.** Pole Figures (PF) of different tubes: (**a**) CA tube, (**b**) CW tube, (**c**) EA tube, (**d**) EW tube.



**Figure 8.** Inverse Pole Figures of different tubes: (**a**) CA tube, (**b**) CW tube, (**c**) EA tube, (**d**) EW tube.

## 4. Discussion

### 4.1. Effect of Extrusion Process on Texture

Texture will be weakened with RE addition [20–22], but the texture is still dependent on the processing parameters [23]. Firstly, deformation temperature is an important factor for the weakening of texture. The dynamic strain-aging (DSA) effect in a narrow window of temperature was proposed by Jiang [23], which indicated that the formation of RE texture components is enhanced by extruding under DSA conditions. This range depends on the type of solute and its concentration, as well as on the combination of extrusion temperature and mean strain rate employed. In this study, the extrusion temperature is selected at 400 °C, which falls in the window of DSA.

Secondly, the cooling rate after deformation would have a significant effect on the formation of texture. Without rapid cooling, a process of static annealing would go through with the residual heat after extrusion. According to previous studies, the process of pre-ferred grain growth is discovered by Wu [16]: in the Mg-1Gd alloy, a gradual strengthening of the <2-1-11> RE-texture component at the expense of the <10-10> component during the recrystallization annealing process. Additionally, the driving force for the preferred grain growth is the difference in stored energy between the <2-1-11> grains and the <10-10> grains. While in the AZ31 alloy, the <2-1-10> component prefers to grow during the recrystallization process. Additionally, the preferred grain growth would be inhibited by the water-cooling method.

In our work, tubes using cast ingots as billet show a higher degree of deflection of peaks on the (0001) pole figure from the deformation axis (also ED). Especially in the CW tube, the peak texture intensity point shows a deflection of 90° from ED. That is because the deformed, unrecrystallized grains in CW tube have the c-axes almost all perpendicular to ED.

As the comparison between air cooling and water cooling (Figure 7), the EA tube shows an obvious texture peak about 60° inclined to ED and the EW tube shows an almost random texture. This is because the preferred grain growth process is inhibited in EW tube during water cooling process.

### 4.2. Effect of Texture on Mechanical Properties

(0001) The basal slip system has the lowest critical resolved shear stress (CRSS) in magnesium, as pervious reported [24,25]. Therefore, the mechanical property depends largely on the grain orientation whether the basal slip is favored or not. In pervious works [26–28], magnesium alloy produced by equal channel angular pressing shows texture with a 45° deflection from the deformation axis, which favors the activation of the basal slip and a good elongation in tension test. In our work, in the EA tube, the peak texture intensity point shows a deflection around 60° from the deformation axis (also ED). In the CA tube, the peak texture intensity point shows a deflection of 80° from ED. Therefore, the activation of the basal slip is much more difficult in the CA tube than in EA during tension along ED, and the CW tube shows a much lower elongation but a higher yield stress (shown in Figure 6).

If texture favors the activation of the basal slip, the tube will achieve a higher elonga-tion. If texture does not favor the activation of the basal slip, the tube will achieve higher yield stress. The result shown in Figure 6 indicated that the EA tube has a higher elongation than the EW tube. It is hard to clarify which tube favors more for the activation of the basal slip. Therefore, Schmid factor analysis is shown in Figure 9. The average Schmid factors of the basal slip system are 0.308 for the CA tube, 0.290 for the CW tube, 0.321 for the EA tube and 0.318 for the EW tube. A high value of Schmid factor distribution can be found in EA, which indicated that activation of the basal slip is more favored in the EA tube during tension tests. Therefore, high elongation was achieved in this tube. A low value of Schmid factor can be found in the CW tube, which indicated that activation of the basal slip is less favored in the CW tube during tension tests. Therefore, low elongation but high yield strength were achieved in this tube. Other factors can also affect mechanical properties,

such as grain size. The EW tube shows a higher average Schmid factor and elongation than the CA tube, which means activation of the basal slip is easier in the EW tube during tension test. However, the yield strength of the EW tube is also higher and this should be caused by a much finer grain size in the EW tube (6.3 μm) than that of the CA tube (26 μm).



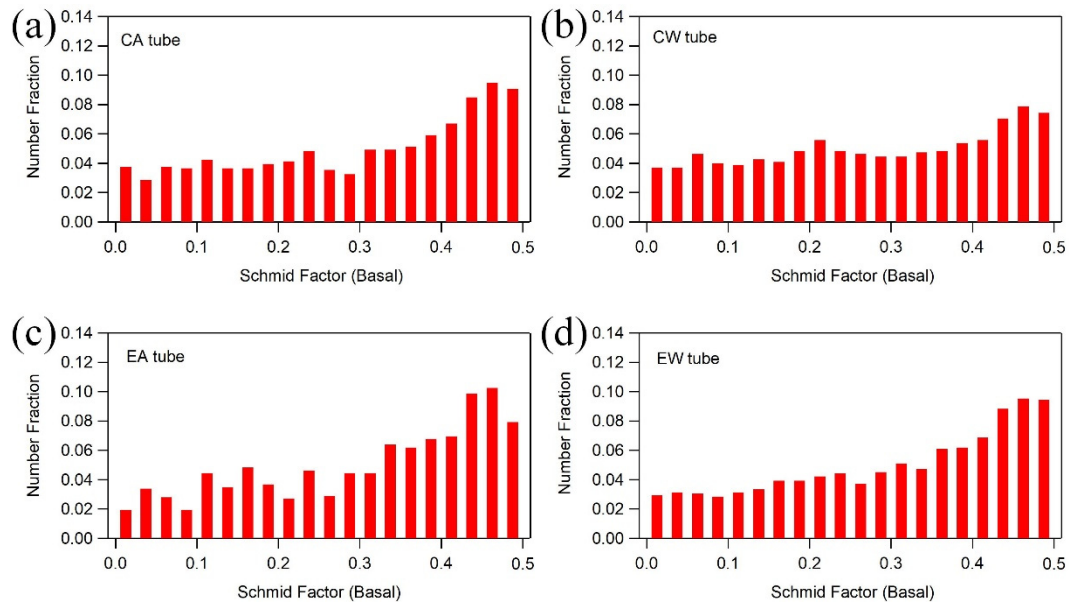**Figure 9.** Schmid factor of basal slip system in (**a**) CA tube and (**b**) CW tube; (**c**) EA tube and (**d**) EW tube.

## 5. Conclusions

In this work, microstructure and mechanical properties of extruded tubes by using traditional extrusion processes and secondary extrusion processes were studied along with different cooling methods. The conclusions of this work are shown as:

(1) A tube using cast ingots as billet and the water-cooling method has a large fraction of unrecrystallized grain with large grain size, which is due to the inhomogeneous deformation during extrusion. Secondary extrusion processes would achieve a fully recrystallized microstructure due to the fine initial grain size.

(2) Tubes using the water-cooling method achieve higher yield stress at around 200 MPa with both cast ingots and extruded bars as billets. This is caused by the fine grain size of these tubes.

(3) Tubes using secondary extrusion processes achieve higher elongation at 28.2% and 23.9% with air-cooling processes and water-cooling processes. This is caused by the extruded texture that favors the activation of the basal slip system.

(4) By using both secondary extrusion processes and the water-cooling method, the extruded texture is almost randomized with the texture intensity of 1.852. This is due to the activation of a more non-basal slip during the extrusion process and the inhibition of preferred grain growth process during the water-cooling process. Both high yield strength (195.3 MPa) and high elongation (23.9%) are achieved in this tube.

**Author Contributions:** Conceptualization, J.S. and J.L.; methodology, J.S. and Q.C.; software, J.L. and L.L.; validation, Y.Z.; formal analysis, J.L.; investigation, J.L.; resources, J.S.; data curation, J.S.; writing—original draft preparation, J.S. and J.L.; writing—review and editing, J.S. and Y.Z.; visualization, J.S.; supervision, J.S.; project administration, J.S.; funding acquisition, J.S. All authors have read and agreed to the published version of the manuscript.

**Conflicts of Interest:** The authors declare no conflict of interest.

## References

1. Mordike, B.; Ebert, T. Magnesium: Properties—Applications—Potential. *Mater. Sci. Eng. A* **2001**, *302*, 37–45. [CrossRef]
2. Luo, A.A. Magnesium: Current and potential automotive applications. *JOM* **2002**, *54*, 42–48. [CrossRef]
3. Luo, A.A.; Wu, W.; Mishra, R.K.; Jin, L.; Sachdev, A.K.; Ding, W. Microstructure and Mechanical Properties of Extruded Magnesium-Aluminum-Cerium Alloy Tubes. *Met. Mater. Trans. A* **2010**, *41*, 2662–2674. [CrossRef]
4. Li, J.; Jin, L.; Dong, J.; Wang, F.; Dong, S. Effects of microstructure on fracture toughness of wrought Mg-8Gd-3Y-0.5Zr alloy. *Mater. Charact.* **2019**, *157*, 109899. [CrossRef]
5. Zhou, B.; Wang, L.; Jin, P.; Jia, H.; Roven, H.J.; Zeng, X.; Li, Y. Revealing slip-induced extension twinning behaviors dominated by micro deformation in a magnesium alloy. *Int. J. Plast.* **2020**, *128*, 102669. [CrossRef]
6. Xin, R.; Liang, Y.; Ding, C.; Guo, C.; Wang, B.; Liu, Q. Geometrical compatibility factor analysis of paired extension twins in extruded Mg–3Al–1Zn alloys. *Mater. Des.* **2015**, *86*, 656–663. [CrossRef]
7. Jin, L.; Mishra, R.K.; Sachdev, A.K. Texture modification during extrusion of some Mg alloys. *Metall. Mater. Trans. A* **2012**, *43*, 2148–2157. [CrossRef]
8. Farzadfar, S.A.; Martin, É.; Sanjari, M.; Essadiqi, E.; Wells, M.A.; Yue, S. On the deformation, recrystallization and texture of hot-rolled Mg–2.9Y and Mg–2.9Zn solid solution alloys—A comparative study. *Mater. Sci. Eng. A* **2012**, *534*, 209–219. [CrossRef]
9. Zhou, N.; Zhang, Z.; Dong, J.; Jin, L.; Ding, W. Selective oxidation behavior of an ignition-proof Mg-Y-Ca-Ce alloy. *J. Rare Earths* **2013**, *31*, 1003–1008. [CrossRef]
10. Zhou, N.; Zhang, Z.Y.; Dong, J.; Jin, L.; Ding, W.J. High ductility of a Mg-Y-Ca alloy via extrusion. *Mater. Sci. Eng.* **2013**, *560*, 103–110. [CrossRef]
11. Fei, H.-J.; Xu, G.-L.; Liu, L.-B.; Bo, H.; Zeng, L.-J.; Chen, C.-P. Phase equilibria in Mg-rich corner of Mg–Ca–RE (RE=Gd, Nd) systems at 400 °C. *Trans. Nonferrous Met. Soc. China* **2013**, *23*, 881–888. [CrossRef]
12. Martin, G.; Sinclair, C.W.; Schmitt, J.H. Plastic strain heterogeneities in an Mg-1Zn-0.5Nd alloy. *Scr. Mater.* **2013**, *68*, 695–698. [CrossRef]
13. Xia, X.; Zhang, K.; Li, X.; Ma, M.; Li, Y. Microstructure and texture of coarse-grained Mg–Gd–Y–Nd–Zr alloy after hot compression. *Mater. Des.* **2013**, *44*, 521–527. [CrossRef]
14. Gao, L.; Luo, A.A. Hot deformation behavior of as-cast Mg–Zn–Mn–Ce alloy in compression. *Mater. Sci. Eng. A* **2013**, *560*, 492–499. [CrossRef]
15. Sanjari, M.; Farzadfar, S.F.; Sakai, T.; Utsunomiya, H.; Essadiqi, E.; Jung, I.H.; Yue, S. Microstructure and texture evolution of MgZnCe magnesium alloys sheets and associated restoration mechanisms during annealing. *Mater. Sci. Eng. A* **2013**, *561*, 191–202. [CrossRef]
16. Wu, W.; Jin, L.; Zhang, Z.; Ding, W.; Dong, J. Grain growth and texture evolution during annealing in an indirect-extruded Mg–1Gd alloy. *J. Alloy. Compd.* **2013**, *585*, 111–119. [CrossRef]
17. Fu, W.; Wang, R.; Xue, H.; Kuang, J.; Zhang, J.; Liu, G.; Sun, J. Effects of Zr addition on the multi-scale second-phase particles and fracture behavior for Mg-3Gd-1Zn alloy. *J. Alloy. Compd.* **2018**, *747*, 197–210. [CrossRef]
18. Liu, Y.; Li, W.; Li, Y.-Y. Microstructure and mechanical properties of ZE10 magnesium alloy prepared by equal channel angular pressing. *Int. J. Miner. Met. Mater.* **2009**, *16*, 559–563. [CrossRef]
19. Yi, S.; Bohlen, J.; Heinemann, F.; Letzig, D. Mechanical anisotropy and deep drawing behaviour of AZ31 and ZE10 magnesium alloy sheets. *Acta Mater.* **2010**, *58*, 592–605. [CrossRef]
20. Stanford, N. The effect of calcium on the texture, microstructure and mechanical properties of extruded Mg-Mn-Ca alloys. *Mater. Sci. Eng. A* **2010**, *528*, 314–322. [CrossRef]
21. Stanford, N. Micro-alloying Mg with Y, Ce, Gd and La for texture modification—A comparative study. *Mater. Sci. Eng. A* **2010**, *527*, 2669–2677. [CrossRef]
22. Stanford, N.; Atwell, D.; Barnett, M.R. The effect of Gd on the recrystallisation, texture and deformation behaviour of magnesium-based alloys. *Acta Mater.* **2010**, *58*, 6773–6783. [CrossRef]
23. Jiang, L.; Jonas, J.; Mishra, R. Effect of dynamic strain aging on the appearance of the rare earth texture component in magnesium alloys. *Mater. Sci. Eng. A* **2011**, *528*, 6596–6605. [CrossRef]
24. Yoo, M.; Wei, C. Slip Modes of Hexagonal-Close-Packed Metals. *J. Appl. Phys.* **1967**, *38*, 4317–4322. [CrossRef]
25. Yoo, M.H. Slip, twinning, and fracture in hexagonal close-packed metals. *Metall. Trans. A* **1981**, *12*, 409–418. [CrossRef]
26. Liu, T. Textures and mechanical behavior of Mg-3.3% Li alloy after ECAP. *Scr. Mater.* **2004**, *51*, 1057–1061. [CrossRef]
27. Del Valle, J.; Carreño, F.; Ruano, O. Influence of texture and grain size on work hardening and ductility in magnesium-based alloys processed by ECAP and rolling. *Acta Mater.* **2006**, *54*, 4247–4259. [CrossRef]
28. Del Valle, J.; Ruano, O. Influence of texture on dynamic recrystallization and deformation mechanisms in rolled or ECAPed AZ31 magnesium alloy. *Mater. Sci. Eng. A* **2008**, *487*, 473–480. [CrossRef]